Local GPS tropospheric tomography

Kazuro Hirahara

Graduate School of Sciences, Nagoya University, Nagoya 464-8602, Japan

(Received December 31, 1999; Revised August 7, 2000; Accepted August 29, 2000)

A formulation of local GPS tropospheric tomography for determining 4-D distribution of refractivity in the troposphere is presented together with a preliminary analysis of local dense GPS campaign data. Dividing the modeling space up to a height of 10 km above GPS receivers into cells, the refractivity in each cell is estimated in a successive time window by a tomographic reconstruction method in a quite similar manner like the seismic velocity in each cell in Earth's interior is estimated in seismic tomography. The basic data for tomography are GPS slant delays for respective pairs of station and satellite, which are the sum of postfit phase residual, hydrostatic and wet slant delay. On the other hand, the slant delay from a station to a satellite is expressed by the summation of the product of path length and refractivity in each cell along the ray path. In a given time window, we have numerous observed slant delays corresponding to different ray trajectories, and the refractivity in each cell can be estimated by discrete inversion and least squares methods. The observational equations are usually singular so that we use a damped least squares method popular in seismic tomography. An example of real data analysis is given for the 1995 Shigaraki GPS campaign data, which reveals the spatial and temporal change of refractivity corresponding to the passage of 'cold front'.

1. Introduction

GPS has recently revealed the detailed crustal deformation with a spatially and temporally high resolution. However, the precision of GPS measurement has still some limitation caused by the excess path delay (EPD) of GPS signal due to the ionosphere (ionosphere refraction) and the neutral atmosphere (tropospheric refraction). EPD in the ionosphere is eliminated to a practical level using a linear combination of dual frequency observables, Lc, but that in the troposphere remains an obstacle preventing high precision in geodesy. Conversely, GPS delay signals include the information of tropospheric structure and can be used to determine the structure, which in turn improves the accuracy of determination of GPS receiver positions. So-called GPS meteorology aims at retrieving the atmospheric structure from the GPS signals and the improvement of geodetic accuracy by utilizing the retrieved atmospheric structure. At present, the tropospheric zenith delays are usually estimated in routine GPS analyses, and the horizontal gradients of tropospheric path delay have recently been included (e.g. Bar-Sever and Kroger, 1998).

In future, a large number of GPS array data will determine both the 4-D tropospheric structure and the positions of receivers. This simultaneous determination procedure will improve both estimates of tropospheric structure and receiver positions, and is therefore a joint goal of GPS meteorology and geodesy. On the other hand, seismic tomography has extensively revealed 3-D velocity structures in the Earth's interior (e.g. Iyer and Hirahara, 1993). In the following, using a reconstruction technique of seismic tomography, we present a tomographic formulation for determining the local 4-D refractivity distribution in the troposphere above a dense array of GPS receivers using the result obtained from a standard GPS analysis, and give an example of real data analysis using GPS data obtained at a dense array of GPS receivers in Shigaraki on November, 1995. Flores *et al.* (2000) have recently presented almost the same formulation of 4-D tropospheric tomography but they used a different solving technique of singular decomposition and Kalman filtering.

2. Formulation of 4-D Tropospheric Tomography

The tropospheric EPD is expressed by

$$\Delta L = \int [n(s) - 1] ds + [S - G]. \tag{1}$$

In the first term, the integral is performed along the line increment ds of straight ray path from a receiver to a GPS satellite, and n is refractive index along the path. The second term indicates the geometric delay due to ray path bending. In seismic tomography, this ray bending effect is so large that the nonlinear inversion is necessary together with 3-D ray tracing. Fortunately, in GPS tomography, this ray bending $[S-G]$ for relatively larger elevation angles which are used in usual GPS analyses is so small that we can ignore (Ichikawa *et al.*, 1995). Accordingly, we can use the straight ray path and a linear inversion, which simplifies the problem than in seismic tomography in this sense.

Usually, instead of the refractive index n, the refractivity N is used and is written as,

$$N = [n - 1]10^6 \tag{2}$$

$$= k_1(P/T) + k_2'(P_v/T)Z_v^{-1} + k_3(P_v/T^2)Z_v^{-1} \tag{3}$$

where P, P_v, T and Z_v are the total atmospheric pressure, the water vapor pressure, the absolute temperature and the compressibility of water vapor, and k_1, k_2' and k_3 are empirical coefficients (e.g. Thayer, 1974). In Eq. (3), the first term and the other terms are called the hydrostatic N_h and wet N_w refractivity. From Eqs. (1) and (3), we get,

$$\Delta L = 10^{-6} \int [N(s)] ds = 10^{-6} \int [N_h(s) + N_w(s)] ds. \quad (4)$$

In the zenith delay ΔL_z which is integrated along the zenith direction in Eq. (4), the first term is called zenith hydrostatic delay, which can be estimated with a sufficient precision from the surface pressure value (Elgered *et al.*, 1991). Dividing the modeling space in the troposphere above receivers into cells as in Fig. 1, and assuming the refractivity is constant within each cell, Eq. (4) is expressed by the summation of cells k along the ray,

$$\Delta L = 10^{-6} \left(N_{st} \Delta S_{st} + \sum_k N_k \Delta S_k \right) \quad (5)$$

where N_{st} and N_k are the refractivity from the receiver to the model space and in cell k, and ΔS_{st} and ΔS_k are the path length from the receiver to the model space and that in cell k, respectively. This is the observational equation for GPS tropospheric tomography, where the unknown parameters are refractivities N_{st} and N_k for each receiver and cell k.

For each epoch, a set of Eq. (5) for pairs of receiver and satellite can be obtained. For a given epoch, a receiver can have only 8–10 satellites on average, and the sufficient path coverage to resolve 3-D distribution of refractivity cannot usually be attained. Therefore, assuming almost constant refractivity values in cells for an appropriate time window, we need to stack all GPS phase data to determine the refractivity distribution in a time window during which satellites move and the sufficient path coverage is possible. Here, we simply determine the distribution of refractivity independently in each time window.

In a time window, we have a set of observational equations of (5), and use a vector notation as

$$\mathbf{d} = G\mathbf{m} \quad (6)$$

where $\mathbf{d}$ is a data vector of EPD, G is a coefficient matrix containing path lengths, and $\mathbf{m}$ is a unknown vector of refractivity. Then, we use a usual damped least squares method popular in seismic tomography (e.g. Hirahara, 1977; Menke, 1984) which minimizes

$$|\mathbf{d} - G\mathbf{m}|^2 + \mathbf{m}^T \Theta \mathbf{m} \quad (7)$$

where $\mathbf{m}^T$ represents the transpose of $\mathbf{m}$, and Θ is a diagonal damping matrix whose i-th diagonal element is the ratio of the variance of data σ_d^2 and a priori variance of i-th parameter σ_{mi}^2. Then we get the solution

$$\mathbf{m}^* = (G^T G + \Theta)^{-1} G^T \mathbf{d} \quad (8)$$

and the resolution matrix R, which gives a measure of resolution of the solution as $\mathbf{m}^* = R\mathbf{m}$, and a model covariance matrix C_m are

$$R = (G^T G + \Theta)^{-1} G^T G \quad (9)$$

$$C_m = \sigma_d^{2*} (G^T G + \Theta)^{-1} G^T G (G^T G + \Theta)^{-1} \quad (10)$$

where

$$\sigma_d^{2*} = |\mathbf{d} - G\mathbf{m}|^2 / (n_d - n_m) \quad (11)$$

and n_d and n_m are the number of data and unknown parameters.

3. Production of Slant EPD as Data for Tomography

Slant EPD, which is a fundamental data set for GPS tomography, was firstly measured by Ware *et al.* (1997). In a standard GPS analysis, the daily position of receiver and the zenith delay for a few hours each are simultaneously estimated using a daily GPS data set. In the usual analysis, assuming a standard atmospheric condition and a model to compute an initial value of zenith delay, the correction for the EPD value is estimated.

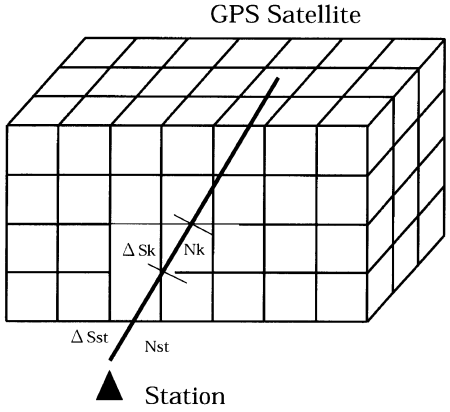

Fig. 1. Divided cells and a ray path from a receiver station to a GPS satellite. N_{st} and N_k are refractivities from the receiver to the model space and in cell k. ΔS_{st} and ΔS_k are the path lengths from the receiver to the model space and in cell k, respectively.

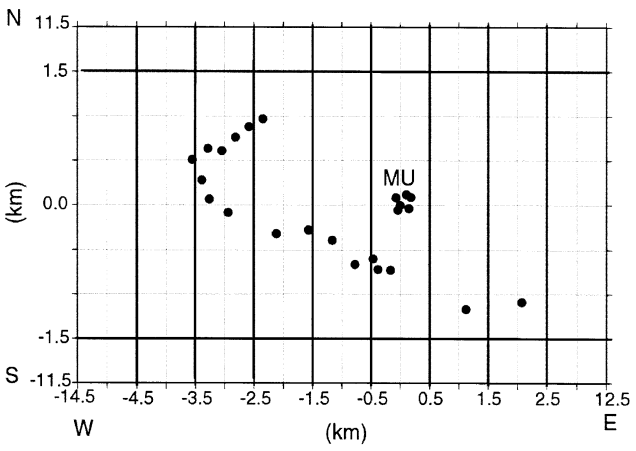

Fig. 2. Horizontal map of the receiver distribution (solid circles) and the cell configuration.

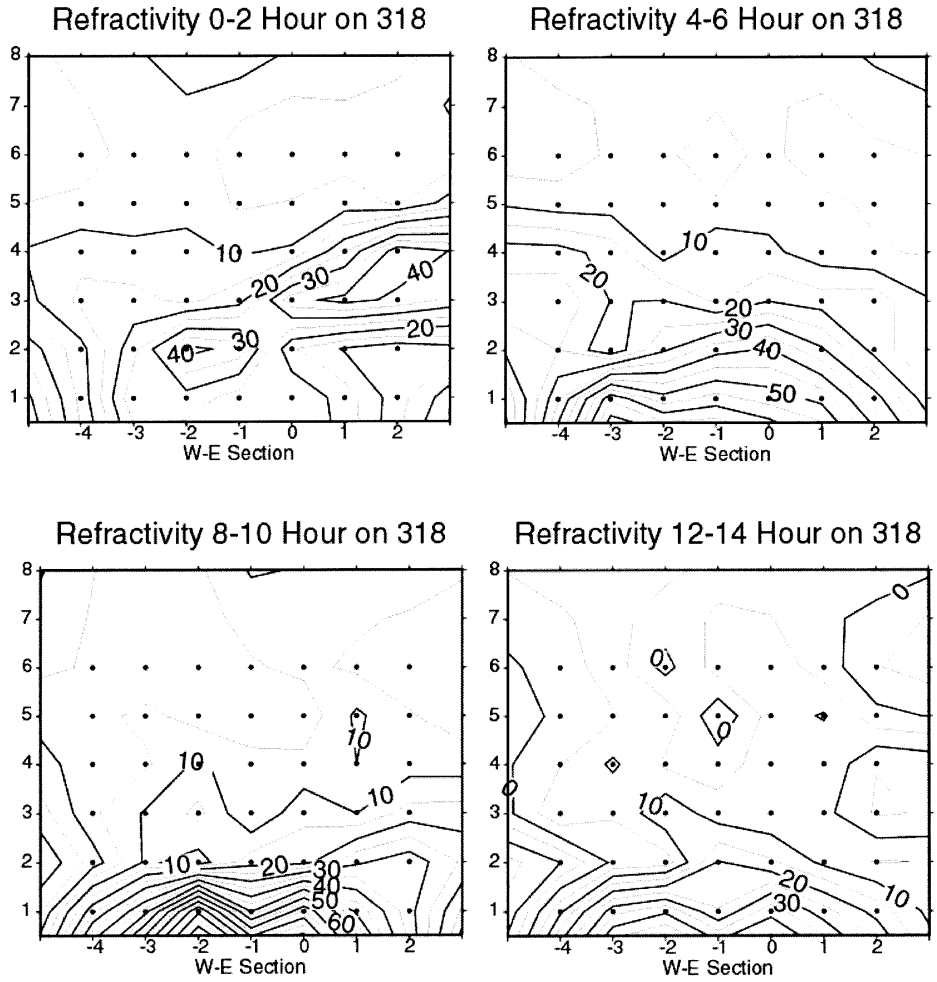

Fig. 3. Distribution of wet refractivity for central cells obtained by tomography in the east-west vertical section for 0–2, 4–6, 8–10 and 12–14 o'clock on day 318. Dots indicate the centers of cells.

We produce the slant EPD from a receiver toward a satellite as,

$$\Delta L = \Delta L_{zho} M_h(\theta) + \Delta L_{zwo} M_w(\theta) + \Delta L_{zc} M_w(\theta) + \Delta L_r. \quad (12)$$

Here, ΔL_{zho}, ΔL_{zwo} and ΔL_{zc} are initial computed value of hydrostatic and wet zenith delays and its estimated correction value, respectively. $M_h(\theta)$ and $M_w(\theta)$ are hydrostatic and wet delay mapping functions for an elevation angle of θ. The last term ΔL_r is the postfit residual EPD which is the difference between the observed phase and the calculated one from the estimated parameters such as the receiver position, the zenith delay and biases in the GPS analysis. The hydrostatic zenith delay derived from the surface pressure value is subtracted from the zenith delay in Eq. (12), and then only the wet delay is obtained.

Equation (5) is for one way phase between a receiver and a satellite. Because an analysis software of GIPSY based on one way phase observational equations, which we employed in this study, produce the phase residual ΔL_r, we use directly this equation. Since other softwares GAMIT and BERNESE employ double difference phase observational equations, the double difference EPD equations for tomography should be used in these cases, though one way phase residuals have recently been calculated for visual inspection of residuals employing sky plot of them. One way EPD has only apparently no clock errors of satellites and receivers, but actually has effects of incorrect estimation of clock biases. Double difference EPD includes completely no clock errors, and hence the data quality is superior to that of one way EPD. However, since four ray paths contribute to one double difference EPD, it may happen that the refractivity values in the cells which are located far away from each other are not well resolved. Thus, one way and double difference EPD have their advantage and disadvantage, and the comparative study of the use of these data will be needed.

4. An Example of Analysis: 1995 Shigaraki GPS Campaign

We briefly describe an example of tropospheric tomography analysis using the 1995 Shigaraki GPS campaign data. On November 13–17 in 1995, a GPS campaign for GPS tropospheric tomography was executed in Shigaraki, where MU radar of Radio Atmospheric Science Center, Kyoto University (34.9°N, 136.1°E), is located. As in Fig. 2, we set 24 GPS dual frequency receivers densely along roads almost in an east-west line with the distance of 6 km, considering the predominant west wind in this season. Actually, the wind

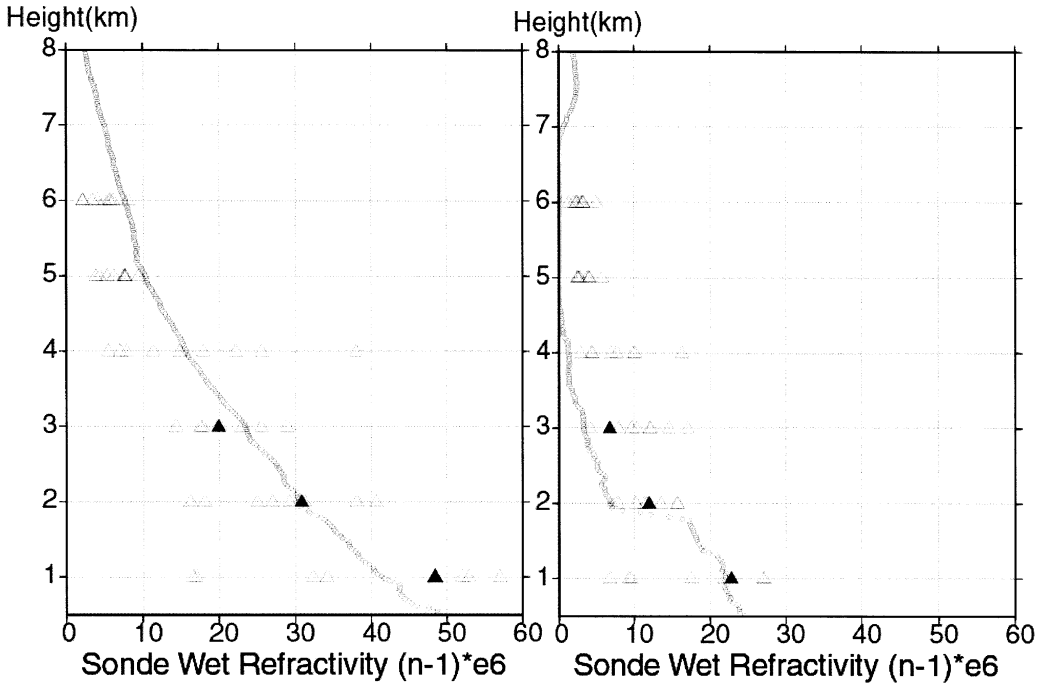

Fig. 4. Comparison of wet refractivity profile for central cells by obtained by tomography for 4–6 o'clock (triangles) and for the radiosonde observation released around 5 o'clock (circles) on day 318 (left) and on 319 (right). Solid triangles represent the refractivity values in cells corresponding to the paths of flying radiosondes.

blew almost from the west to the east throughout the period of observation. All stations were located between 300–500 m in height. The elevation cut-off angles were set to be 15 degrees, but the actual elevation angles for the observed satellites were larger because of site conditions in the field. Because of power supply, the GPS observations at 11 sites using battery were made for 8 hours (0–8 UT), while the continuous observations were made at the other GPS sites. Since the GPS observations were intensively executed on two days, 14th and 15th (day 318 and 319), we analyzed these data. We made some radiosonde observations at the site close to the MU radar site, and we can compare the tomographic result of refractivity with the refractivity profiles by radiosonde.

We use Precise Point Positioning (PPP) of GIPSY to determine the tropospheric zenith delays and postfit residuals for each 5 minutes, because we employ the satellite clock values determined for each 5 minutes by JPL global analyses. Then we produce slant wet delays by subtracting hydrostatic zenith delays from the zenith delays in Eq. (12) for each 5 minutes.

The cold front passed by around noon on day 318, and then the rain stopped and the clear sky appeared later. Correspondingly, the estimated zenith delay corrections were changing from about 17 cm at 0–10 o'clock to 9 cm at noon on day 318 and remained to be a level of 8–10 cm later.

We set the configuration of $9 \times 3 \times 7$ cells in Fig. 2. The size of central east-west cell is $1 \times 3 \times 1 \sim 3.5$ km, and that of peripheral cells is $1 \sim 10 \times 10 \times 1 \sim 10$ km. We divide 2-day data into 24 time windows with 2 hours and estimate the refractivity distribution in each time window. Since the peripheral cell size is large, we use the following large damping values. Assuming a priori uncertainties of $\sigma_d = 5$ cm, $\sigma_{mst} = 3$ cm for receiver refractivity, $\sigma_{mcell} = 0.9$ cm for cell refractivity, we use the values of diagonal element of damping matrix, 3.0 and 30.0 for receiver and cell refractivity, respectively. The average sizes of slant delays, the postfit residuals of GIPSY, and the residuals after refractivity tomography are 23.76 cm, 1.02 cm and 0.68 cm for day 318, and 14.04 cm, 0.96 cm and 0.59 cm for day 319, respectively. Thus, we could get smaller residuals by introducing 4-D refractivity variations. In spite of large damping values used, most of central east-west cells have the diagonal elements of resolution matrix greater than 0.7, indicating a good resolution of the central cells. Accordingly, we show the results only for central cells.

Figures 3 show the distribution of refractivity in the east-west vertical section for central cells for the time window of 0–2, 4–6, 8–10, 12–14 o'clock on day 318. As the cold front was passing, the wet air with high refractivity was downgoing and the air became dry. The wet refractivity distribution remained at small values and was not so variable after the passage of the cold front. Finally, we show the comparison of the refractivity distribution by tomography with the refractivity profile by radiosonde observation. Figure 4 shows the comparison of refractivity profile for central cells for 4–6 o'clock and for radiosonde observation released around 5 o'clock on day 318 and 319, respectively. Especially, the wet refractivity values in the cells corresponding to the paths of radiosondes are marked by solid triangles. This indicates the wet refractivity distribution obtained by GPS tomography agrees well with the radiosonde observations.

5. Discussions and Conclusions

As in seismic tomography, we present a formulation of local GPS tropospheric tomography and a way to produce slant

EPD as tomographic data using processed GPS data. There are other regularization techniques such as an introduction of smoothness criterion in solving singular normal equations. Or, if we have a priori information on refractivity distribution $\mathbf{m}_o$ derived from other observations such as frequent radiosonde observations, we would have a better imposed closeness to this a priori distribution: $(\mathbf{m} - \mathbf{m}_o)^T C_{mo}^{-1}(\mathbf{m} - \mathbf{m}_o)$ instead of the second term in Eq. (7), where C_{mo} is a priori covariance matrix of $\mathbf{m}_o$. The smoothness in the time domain or Kalman filter-like approaches as in Flores *et al.* (2000) may be introduced in future, though we simply inverse independently in a successive time window here.

While our approach is very simple, the local GPS tropospheric tomography is very hopeful for retrieving small scale 4-D refractivity structure. The application of our approach to GPS data of the 1995 Shigaraki GPS campaign has provided temporal and spatial properties of a passing cold front.

Acknowledgments. I thank Torao Tanaka and other members who took part in the 1995 Shigaraki GPS campaign for allowing the use of data and discussions on GPS tropospheric tomography. My thanks are due to Toshitaka Tsuda and Takayuki Yoshihara for providing with radiosonde data and their helpful discussions. Two anonymous reviewers' comments significantly improved the manuscript. This study was funded by 'GPS meteorology project' of Science and Technology Agency.

References

Bar-Sever, Y. E. and P. M. Kroger, Estimating horizontal gradients of tropospheric path delay with a single GPS receiver, *J. Geophys. Res.*, **103**, 5019–5035, 1998.

Elgered, G., J. L. Davis, T. A. Herring, and I. I. Shapiro, Geodesy by radio interferometry: water vapor radiometry for estimation of the wet delay, *J. Geophys. Res.*, **96**, 6541–6555, 1991.

Flores, A., G. Ruffini, and A. Ruis, 4D tropospheric tomography using GPS slant wet delays, *Annales Geophys.*, **18**, 223–234, 2000.

Hirahara, K., A large-scale three-dimensional seismic structure under the Japan Islands and the Sea of Japan, *J. Phys. Earth*, **25**, 393–417, 1977.

Ichikawa, R., M. Kasahara, N. Mannoji, and I. Naito, Estimations of atmospheric excess path delay based on three-dimensional numerical prediction model data, *J. Geod. Soc. Japan*, **41**, 379–408, 1995.

Iyer, H. M. and K. Hirahara, *Seismic Tomography*: *Theory and Practice*, Chapman and Hall, 842 pp., 1993.

Menke, W., *Geophysical Data Analysis*: *Discrete Inverse Theory*, Academic press, 260 pp., 1984.

Thayer, D., An improved equation for the radio refractive index of air, *Radio Sci.*, **9**, 803–807, 1974.

Ware, R. H., C. Alber, C. Rocken, and F. Solheim, Sensing integrated water vapor along GPS ray paths, *Geophys. Res. Lett.*, **24**, 417–420, 1997.

K. Hirahara (e-mail: hirahara@eps.nagoya-u.ac.jp)